

# Minimum in the pressure dependence of the interfacial free energy between ice Ih and water

P. Montero de Higes<sup>1</sup>, J. R. Espinosa<sup>2</sup>, C. Vega<sup>2</sup>, and C. Dellago<sup>1,\*</sup>

<sup>1</sup>*Faculty of Physics, University of Vienna, A-1090 Vienna, Austria*

<sup>2</sup>*Departamento de Química Física, Facultad de Ciencias Químicas, Universidad Complutense de Madrid, 28040 Madrid, Spain*

Despite the importance of ice nucleation, this process has been barely explored at negative pressures. Here, we study homogeneous ice nucleation in stretched water by means of Molecular Dynamics Seeding simulations using the TIP4P/Ice model. We observe that the critical nucleus size, interfacial free energy, free energy barrier, and nucleation rate barely change between isobars from -2600 to 500 bar when they are represented as a function of supercooling. This allows us to identify universal empirical expressions for homogeneous ice nucleation in the pressure range from -2600 to 500 bar. We show that this universal behavior arises from the pressure dependence of the interfacial free energy which we compute by means of the mold integration technique finding a shallow minimum around -2000 bar. Likewise, we show that the change in the interfacial free energy with pressure is proportional to the excess entropy and the slope of the melting line, exhibiting the latter a reentrant behavior also at the same negative pressure. Finally, we estimate the excess energy and the excess entropy of the ice Ih-water interface.

\*christoph.dellago@univie.ac.at

## I. INTRODUCTION

Water crystallization is an essential phase transition in nature and technology. However, in the cryopreservation of biological samples [1, 2], ice formation can be disastrous. The low temperature preserves the biological material but causes the water within the sample to be in a metastable state subject to crystallization [3]. Interestingly, by keeping the sample under high pressure, ice nuclei are less likely to form keeping water liquid for a longer time [4–6]. The frequency of the nucleation process is mainly determined by the thermodynamic driving force and the cost of creating the interface between the emerging nucleus and the metastable liquid. The reason why high pressure slows down the nucleation process is that the difference in chemical potential between ice and water,  $\Delta\mu$ , which represents the thermodynamic driving force, barely changes between isobars whereas the cost of creating the interface notably increases [7]. The interfacial free energy is the variable that quantifies this cost. At coexistence, through a planar interface, the interfacial free energy  $\gamma_m$  differs from the value for a critical nucleus  $\gamma$  due to the curvature of the surface [8]. Nevertheless, both notably increase at high pressure [7].

Homogeneous ice nucleation at standard and high pressure has been extensively explored [7, 9–19]. However, ice nucleation in water under negative pressure, i.e. stretched water, has caught less attention [20–22]. This process is relevant in porous media containing water solutions [23] and also in water transpiration inside plants [24] where negative pressure occurs. Creating and maintaining negative pressure over a sample is non-trivial in experiments [25]. This is because a liquid at negative pressure is metastable [26, 27]. In general,

this metastability is considered with respect to the vapor phase [28, 29], although at certain conditions, it can be also metastable with respect to ice. Some ingenious approaches to create negative pressure in metastable water include the use of a Berthelot tube [30], centrifugation [31], and more recently the use of acoustic waves [25, 29, 32]. In contrast, in computer simulations is straightforward to work under negative pressures.

In this work, we investigate how ice nucleation properties are affected by negative pressure at different degrees of supercooling. In fact, we find little effect when pressure changes from strongly negative to moderately positive. We investigate the role of the interfacial free energy since it is a key property in determining the phase behavior of water at high pressure [7]. We find that the slope of the melting line is crucial to describe the change with pressure of the interfacial free energy which displays a shallow minimum at negative pressure. Our study is based on molecular dynamics simulations with the TIP4P/Ice model [33] which has been extensively used to describe ice nucleation [7, 9, 12, 21] and growth [34, 35] as well as in supercooled water [36, 37]. In particular, we employ the seeding technique [9, 38] to study nucleation and the mold integration technique [39] to measure the interfacial free energy at coexistence.

## II. SIMULATION METHODS

All simulations have been done with the GROMACS package (4.6.7-version in double precision) with the TIP4P/Ice water model. The simulations are performed in the isothermal-isobaric (NpT) ensemble with a time step of 2 fs using the Nose-Hoover thermostat [40, 41] and the Parrinello-Rahman barostat [42] both with a relaxation time of 0.5 ps. Electrostatic interactions are

accounted for via the particle-mesh-Ewald summation algorithm [43] with order 4 and a Fourier spacing of 0.1 nm. The cutoff for the Lennard-Jones and the Coulombic interactions is set to 0.9 nm and long-range corrections to the Lennard-Jones part of the potential are included in energy and pressure.

To study nucleation we use the seeding technique [9, 44, 45] which involves the combination of molecular dynamics simulations and Classical Nucleation Theory (CNT) [46, 47]. This technique is based on the behavior of a critical nucleus which has equal probability of growing and melting when surrounded by the metastable phase at the critical pressure and temperature. In practice, one inserts a spherical ice-Ih seed in metastable water and then keeps track of the time evolution of the size of the cluster. One can vary  $T$ ,  $p$  and the seed size in order to find at which conditions a certain nucleus size is critical ( $N_c$ ). Once  $N_c$  is known, CNT is used to find the interfacial free energy  $\gamma$ , the barrier height  $\Delta G_c$ , and the nucleation rate  $J$ . Our system sizes ranged between 80000 and 250000 water molecules in total. The duration of the trajectories is between 40 and 115 ns.

It is important to note that in the Gibbsian description of interfaces, one has two bulk phases separated by a dividing surface. However, there is some arbitrariness in the location of the dividing surface which also affects to the interfacial free energy  $\gamma$  when the interface has curvature [48–51]. Within the CNT framework, the relevant dividing surface is the surface of tension [52, 53]. In order to find the surface of tension we employ an empirical approach that has been successfully applied in crystal nucleation for a large variety of systems [7, 21, 38, 39, 54, 55]. In this approach, the averaged Steinhardt bond order parameter [56],  $\bar{q}_6(T, p)$  is used in combination with the mislabelling criterion [9] to identify ice-like and water-like molecules. Within a cutoff distance of 3.5 Å, we obtain  $\bar{q}_6(T, p)$  for each molecule. The molecules with  $\bar{q}_6(T, p)$  above a certain threshold  $q_{6,t}(T, p)$  are labeled as ice whereas those below are labeled as liquid. This threshold depends weakly on the considered thermodynamic range covering pressures from -2600 to -1000 bar and temperatures from 250 to 270 K (see the supplementary material in Ref. [21] for the isothermal change in  $q_{6,t}(T, p)$  with pressure). In this work, the value changes between 0.365 for the highest temperature and pressure to 0.385 for the lowest temperature and pressure.

Once  $N_c$  is known, we employ the CNT equations [46, 47] to determine other important parameters. The interfacial free energy  $\gamma$  is given as

$$\gamma = \left( \frac{3N_c \rho_{ice}^2 |\Delta\mu|^3}{32\pi} \right)^{1/3}, \quad (1)$$

where  $N_c$  is the size of the critical nucleus,  $\rho_{ice}$  is the

number density of ice-Ih in the bulk at the metastable conditions at which the nucleus is critical, and  $|\Delta\mu|$  is known as the driving force to nucleation, i.e. the difference in chemical potential between the liquid and ice phases at the conditions which cause the nucleus to be critical. This property can be obtained by thermodynamic integration along an isobar [57],

$$\left| \frac{\Delta\mu}{k_B T} \right| = \left| \int_{T_m}^T \frac{1}{k_B T^2} \left( \frac{H_{ice}}{N_{ice}} - \frac{H_w}{N_w} \right) dT \right|, \quad (2)$$

where  $k_B$  is the Boltzmann constant,  $T_m$  is the melting temperature, and  $H$  the enthalpy, which can be obtained from simulations of bulk ice-Ih and bulk water along the isobar of interest.

Then, the free energy barrier is given as

$$\Delta G_c = \frac{16\pi\gamma^3}{3\rho_{ice}^2 |\Delta\mu|^2} = \frac{N_c |\Delta\mu|}{2}, \quad (3)$$

which allows us to obtain the nucleation rate  $J$ , the number of critical nuclei forming per unit of time and volume. According to CNT,  $J$  is given as

$$J = \rho_w \sqrt{\frac{|\Delta\mu|}{6\pi k_B T N_c}} f^+ \exp\left(-\frac{\Delta G_c}{k_B T}\right), \quad (4)$$

where  $f^+$  is the attachment rate which can be approximated through this expression [7, 21]

$$f^+ = \frac{24D_w N_c^{2/3}}{\lambda^2}, \quad (5)$$

where  $D_w$  is the diffusion coefficient of the metastable liquid and  $\lambda$  is a characteristic length, the typical distance that a water molecule covers in order to attach into the nucleus, whose value is approximately 3.8 Å for water [7, 21].

To find the ice-Ih-water interfacial free energy at coexistence for a planar interface,  $\gamma_m$ , we use the mold integration technique [39], which consists in computing the reversible work  $W$  that is necessary to form a crystal slab within a liquid at coexistence. This work is related to the interfacial free energy at coexistence,  $\gamma_m$ , by  $W = 2A\gamma_m$  where  $A$  is the interfacial area and the number 2 accounts for the two interfaces of the slab. The slab formation is induced by switching on an attractive interaction between the mold of potential energy wells and the particles of the initial liquid. The wells are arranged in the equilibrium positions of the oxygen atoms in the ice facet under investigation at coexistence conditions, i.e. for temperatures and pressures located along the ice Ih-water equilibrium line for the TIP4P/Ice water model. First, one has to obtain  $\gamma_{rw}$ , which is given as

$$\gamma_{r_w} = \frac{1}{2A} \left( \epsilon_w N_w - \int_0^{\epsilon_w} \langle N(\epsilon) \rangle d\epsilon \right), \quad (6)$$

where  $r_w$  indicates the radius of the potential wells and  $\epsilon$  is their energy (with maximum depth equal to  $\epsilon_w$ ).  $N_w$  is the number of wells in the mold and  $\langle N(\epsilon) \rangle$  is the average number of occupied wells at a given potential depth  $\epsilon$ . The integration needs to be reversible. To ensure this, thermodynamic integration is performed for wells whose radius is larger than a certain value  $r_w^0$ . At  $r_w^0$  the slab is fully formed and the stability no longer depends on the mold-liquid interactions, hence, leading to potentially irreversible ice growth. However, since this is the radius that recovers the actual value of  $\gamma_m$ , thermodynamic integration is repeated for several values of  $r_w < r_w^0$  and then  $\gamma_{r_w}$  is extrapolated to its value at  $r_w^0$  giving  $\gamma_m$  [39].

### III. RESULTS

#### A. Universality in ice nucleation variables at negative and moderate pressure

First, we study nucleation along the isobars of -2600, -2000, and -1000 bar by means of the seeding approach. For pressures below -3000 bar we observed spontaneous cavitation occurring within the time scale of the trajectories needed in the seeding method. We obtain the critical nucleus size  $N_c$ , the driving force to nucleation  $|\Delta\mu|$ , the interfacial free energy  $\gamma$ , the free energy barrier to nucleation  $\Delta G_c$  and the nucleation rate  $J$ . These results are presented in Table I. As can be seen, even though the pressure significantly differs, the results are surprisingly similar for nuclei of similar size for equivalent supercoolings. This behaviour is considerably different from what has been found when comparing the nucleation scenario of normal vs. high pressure (i.e. 2000 bar; Ref. [7]), where the increase in pressure brings down the ice nucleation rate.

To further understand this behavior, we connect our results with those from previous works where nucleation had been studied for the TIP4P/Ice model at different pressures including negative, moderate, and high pressure states [7, 21]. In Fig. 1 a) we show the critical nucleus size as a function of supercooling for several isobars. We provide results at moderate supercoolings at -2600, -2000, and -1000 bar. For these same isobars as well as for the 1 bar isobar, we show the values reported in Ref. [21]. For the 1 bar isobar, we also show the values given in Ref. [7], which also provides with the values at the 2000 bar isobar. As can be seen, only the points corresponding to the 2000 bar isobar [7] exhibit a different trend. The isobars at -2600, -2000, and -1000 bar from this work as well as from Ref. [21], and the 1 bar isobar from both Refs. [7, 21] follow approximately

the same curve. Notice that even a point at 450 bar reported in Ref. [21] was included being in agreement with this group of isobars. In fact, as shown in Fig. 1 b), pressure hardly affects the nucleation free energy barrier as a function of supercooling from -2600 bar to 450 bar.

Our results from Fig. 1 suggest that a similar nucleation behaviour as a function of supercooling may take place from -2600 to 450 bar. That is a strikingly different behavior to the one observed when increasing pressure to 2000 bar. Thus, we propose universal empirical expressions for the variation of different homogeneous ice nucleation properties with the supercooling independently of the pressure as long as it is within this regime. Nevertheless, we first need to confirm that what was observed for  $N_c$  and  $\Delta G_c$  also applies to  $J$ . In Fig. 2 we show again a)  $N_c$  and b)  $\Delta G_c$  as well as c)  $\gamma$  and d)  $\log_{10} J$ . This time, for each magnitude, we include a common fit to data from moderately positive to deeply negative pressure (including our own data and those from Refs. [7, 21]) along a separate fit at high pressure [7]. In c) we show  $\gamma$  which exhibits higher variance. Finally, in d), we show how very different pressures (from largely negative to moderately positive) lead to approximately the same nucleation rate  $J$  as a function of supercooling,  $\Delta T = T_m - T$ . The values of  $T_m$  are given in Table II. Hence, we can use the respective common fit as universal empirical expressions to describe the change with supercooling within this broad range of pressures.

For  $N_c$  we obtain

$$N_c(\Delta T) = 1.2 \cdot 10^7 \cdot \left( \frac{\Delta T}{T_0} \right)^{-2.8} \quad (7)$$

and for  $\Delta G_c$  (in kJ/mol)

$$\Delta G_c(\Delta T) = 2.3 \cdot 10^5 \cdot \left( \frac{\Delta T}{T_0} \right)^{-2.1}, \quad (8)$$

where  $T_0$  equals 1 K for correctness of units. For  $\gamma$  in  $\text{mJ/m}^2$ , we obtain

$$\gamma(\Delta T) = 26.6 - 0.174 \cdot \Delta T, \quad (9)$$

and, finally, for  $J$  in  $\text{m}^{-3} \text{s}^{-1}$ , one should use Eq. 4 along with Eq. 8 (after converting into  $k_B T$  units), and  $10^{36} \text{ m}^{-3} \text{s}^{-1}$  as the prefactor  $(\rho_w \sqrt{|\Delta\mu| / (6\pi k_B T N_c)} f^+)$ .

The results shown in Fig. 2 have interesting consequences. First, taking into account that  $N_c$  and  $\gamma$  (panels a) and c) respectively) are roughly independent of  $p$  when it goes from largely negative to moderately positive pressures, the isobaric Tolman length which determines the change in  $\gamma$  with the inverse of the radius of curvature of the cluster along an isobar [8, 58, 59] is

$N_c$	$T$ [K]	$\Delta T$ [K]	$p$ [bar]	$\rho_w$ [g/cm <sup>3</sup> ]	$\rho_{ice}$ [g/cm <sup>3</sup> ]	$ \Delta\mu $ [kJ/mol]	$\gamma$ [mJ/m <sup>2</sup> ]	$\Delta G_c$ [kJ/mol]	$\log_{10}(J)$ [m <sup>-3</sup> s <sup>-1</sup> ]
1650	255	23	-1000	0.9208	0.8999	0.367	21.62	303	-24
7450	264	14	-1000	0.9285	0.8985	0.237	23.03	883	-136
1750	255	25	-2000	0.8855	0.8916	0.367	21.87	321	-28
7600	266	14	-2000	0.8876	0.8894	0.224	21.74	850	-128
1950	255	24	-2600	0.8674	0.8866	0.340	20.89	332	-30

TABLE I. Seeding results in tabular form.  $N_c$  is the critical nucleus size,  $T$  and  $p$  are the thermodynamic conditions that make such nucleus size to be critical, and  $\Delta T$  is the supercooling,  $T_m - T$ . The densities of water  $\rho_w$  and ice  $\rho_{ice}$  are also shown, as well as the interfacial free energy at nucleation  $\gamma$ , the barrier height  $\Delta G_c$ , and the base-10 logarithm of the nucleation rate  $\log_{10}(J)$ .

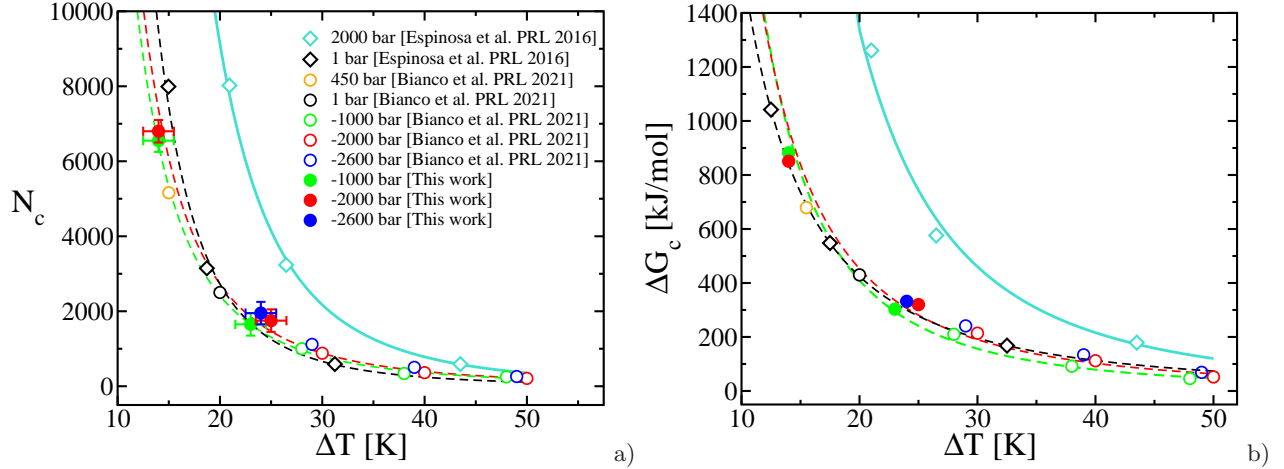


FIG. 1. a) Critical nucleus size and b) free energy barrier to undergo nucleation against supercooling. The same legend applies in both panels. Numerical details can be seen in Table I. The color indicates the pressure, whereas solid symbols correspond to simulations performed in this work, and empty symbols correspond to data obtained from previous work as indicated in the legend. For the same pressure but different work we use different symbols. The lines are power law fits to points sharing the same pressure independently on the work in which they were obtained.

roughly constant too and equal to 0.24(5) nm, where the parenthesis indicates uncertainty in the last digit. This result is in agreement with previous work [54]. Second, in panel d) one can see that from strongly negative to moderately positive pressure we obtain the same nucleation rate with respect to the supercooling which means that the homogeneous nucleation line (HNL) should be at a constant distance to the melting line in this regime as predicted recently for this water model [21] as well as for the mW model [60] in Ref. [22]. In Fig. 3 we show the estimates for the model [7, 21] assuming that the HNL corresponds to an iso-nucleation rate of  $\log_{10} J / (\text{m}^{-3}\text{s}^{-1}) = 15$  and we compare it to the experimental HNL [4]. Also, the coexistence lines of the model [21] and the experimental one [20] are presented showing how the distance between the coexistence line and the HNL is roughly constant until pressure increases enough such that the required supercooling to reach  $\log_{10} J = 15$  becomes larger. However, even though this result might be useful, a physical explanation is still missing. In order to answer this question, we look at the pressure-induced deceleration of ice nucleation. In

2016, Espinosa et al. [7] showed that the origin of this phenomenon arises from the increase with pressure of the interfacial free energy both at coexistence  $\gamma_m$  and for nucleation ( $\gamma$  at a given supercooling  $\Delta T$ ) while the difference in chemical potential  $\Delta\mu$  does not change so much with  $\Delta T$ . Thus, one needs a larger  $\Delta T$  to obtain the same  $J$  at high pressure. In this work, we observe approximately the same  $J$  as a function of  $\Delta T$  from strongly negative to moderately positive pressure.

Since we obtain roughly the same  $\gamma$  as a function of  $\Delta T$  at different negative pressures, we expect also  $\gamma_m$  to barely change with  $p$ . The term  $\gamma_m$  refers to a planar interface between ice and water at certain conditions along the coexistence line whereas the term  $\gamma$  refers to a curved interface between a critical nucleus of ice and water at a certain supercooling  $\Delta T$  along an isobar. In both cases, thermodynamic equilibrium holds. However, when the interface is planar then the pressure is equal in both phases while in a spherical interface the pressure changes between phases following the Young-Laplace equation. Then, we compute  $\gamma_m$

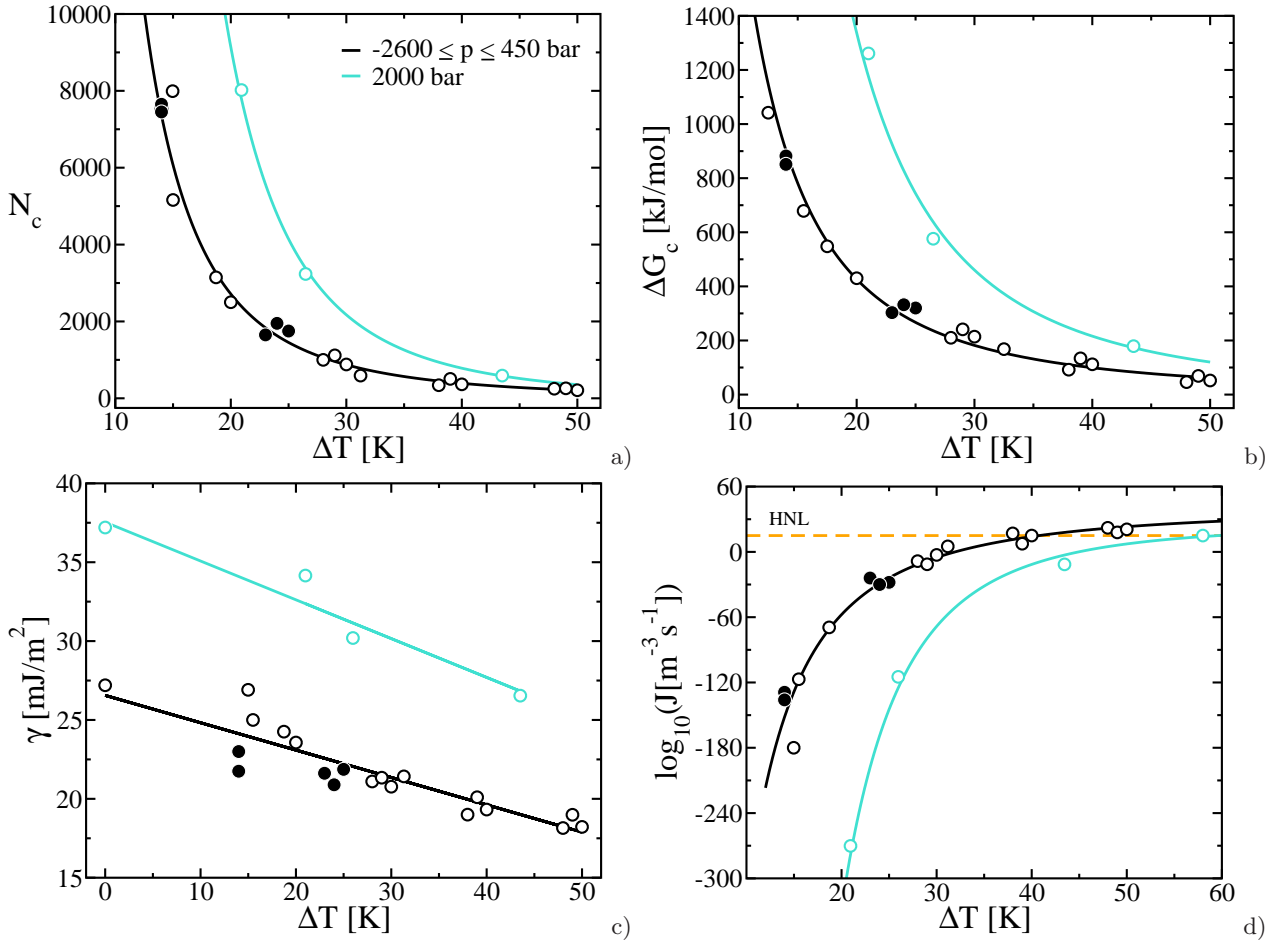


FIG. 2. a) Critical nucleus size, b) nucleation free energy barrier, c) interfacial free energy, and d)  $\log_{10} J$  against supercooling. The same legend applies to all panels. The color indicates the pressure regime according to the legend. Points obtained in this work are shown as solid symbols whereas results from Refs. [7, 21] as empty symbols. Black solid symbols are restricted to pressures between -2600 and -1000 bar, whereas black empty symbols cover from -2600 up to 450 bar. Cyan empty symbols correspond to 2000 bar. For each magnitude, a common fit to our data and those of Refs. [7, 21] is included. For panels a) and b) a power law fit is used as given by Eq. 7 and Eq. 8 respectively, whereas for panel c) we use a linear fit (Eq. 9) and for panel d) we use a CNT-based fit. HNL in panel d) is the iso-nucleation line of  $\log_{10}(J[m^{-3}s^{-1}]) = 15$ .

for several points. In addition to the negative pressure isobars, we compute two points at 1000 bar and 2000 bar respectively. We study only the basal plane as we do not expect severe anisotropy (as much as  $\sim 10\%$ ) with the prismatic ones [39, 61–63]. The results are presented in Table II and in Fig. 4. As shown,  $\gamma_m$  barely changes along the coexistence line when  $p$  varies from strongly negative to moderately positive. Interestingly,  $\gamma_m$  displays a shallow minimum. Thus, as long as  $\Delta\mu$  does not change significantly with  $\Delta T$  at negative  $p$ , one can explain why in Fig. 2,  $N_c$ ,  $\Delta G_c$ ,  $\gamma$ , and  $J$  seem to be independent of  $p$  against the supercooling when  $p$  is negative or moderate. In order to confirm this, we evaluate the effect of  $p$  on  $\Delta\mu$  as a function of supercooling  $\Delta T$  by comparing with the value at 1 bar. To do so, we compute  $(\Delta\mu_p - \Delta\mu_1)/\Delta\mu_1$  for the different isobars  $p = -2600, -2000, -1000, 1, 2000$  bar as a function of  $\Delta T$  (for 1 and 2000 bar we use the

data from Ref. [7]). As can be seen in Fig. 5 a), the 2000 bar isobar is very similar to the -1000 bar one in terms of  $\Delta\mu$  with respect to  $\Delta\mu_1$ , and the -2600 bar is the one that deviates the most with up to 18%. This deviation is however compensated in  $\gamma$  which is rather dispersed and in the end  $N_c$ ,  $\Delta G_c$ , and  $J$  are very well described by universal empirical expressions. Moreover, in Fig. 5 b), we show  $\Delta G$  obtained as  $N_c|\Delta\mu|/2$  by setting  $N_c$  to the common fit of Eq. 7 and changing  $\Delta\mu$  to that of the different isobars. As can be seen, from strongly negative to moderately positive pressure, the change in  $\Delta\mu$  does not significantly affect the free energy barrier for isobars between -2600 to 450 bar. Thus, we confirm that the universality in nucleation properties presented in Fig. 1 and Fig. 2 is the consequence of the small variation with  $p$  of the difference in chemical potential  $\Delta\mu$  as well as in the interfacial free energy both at coexistence  $\gamma_m$  and for the nucleation  $\gamma$  at a given  $\Delta T$ .

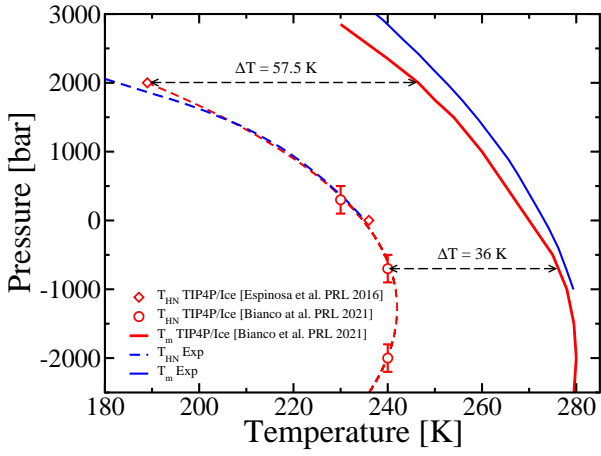


FIG. 3. In solid lines, the coexistence lines  $T_m$  where blue is experimental [20] and red is for the TIP4P/Ice [21]. The dashed blue line corresponds to the experimental HNL [4]. Empty red symbols correspond to simulation estimates for the TIP4P/Ice of the HNL for  $\log_{10} J/(m^{-3}s^{-1}) = 15$  (the dashed red line is a guide connecting these points). The turning point of the melting curve of TIP4P/Ice occurs at 280K and -2000 bar.

$p_m$ [bar]	$T_m$ [K]	$\gamma_m$ [mJ/m <sup>2</sup> ]
-2600	279.0	27.1(1.5)
-2000	280.0	26.5(1.5)
-1000	278.0	25.6(1.5)
1	270.0	27.2 (0.8)
1000	260.0	29.0(1.5)
2000	246.5	37.2(1.5)

TABLE II. Interfacial free energy  $\gamma_m$  at different  $T-p$  points of the coexistence line for the basal plane. Value at 1 bar is from Ref. [39].

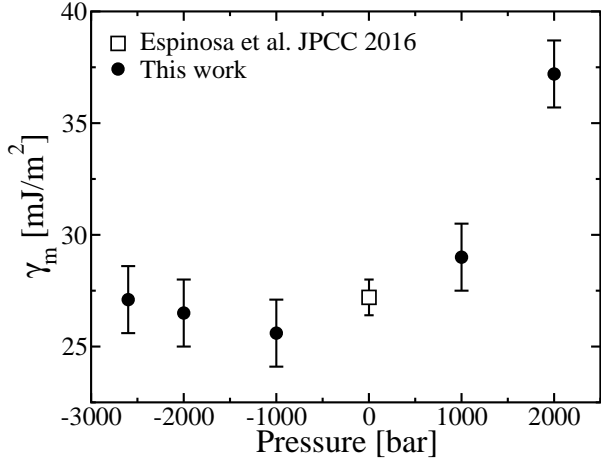


FIG. 4. Ice Ih-water interfacial free energy at coexistence for the basal plane for the TIP4P/Ice model.

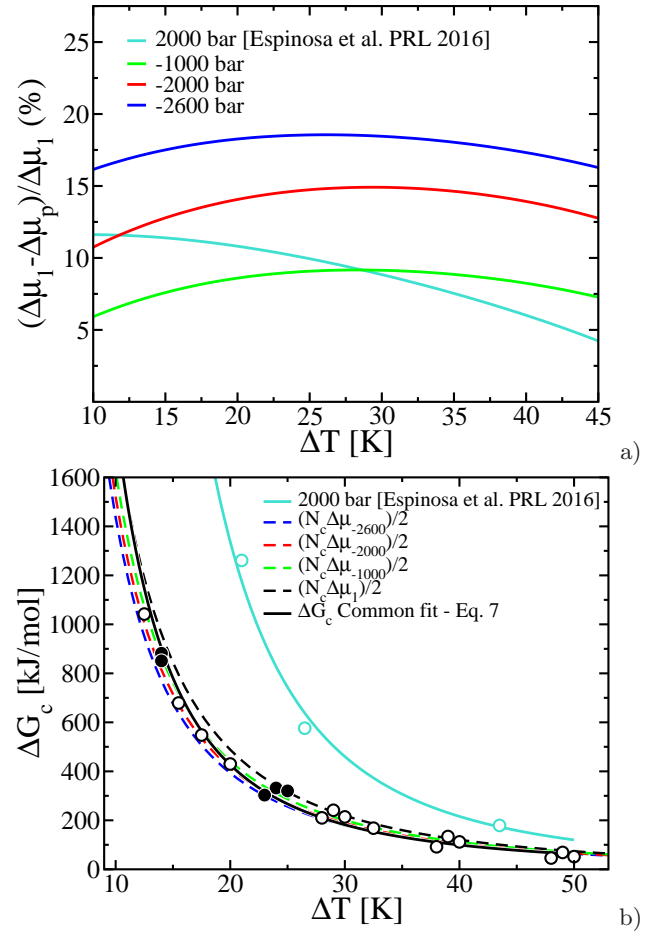


FIG. 5. a) Deviation in  $\Delta\mu$  at different isobars (-2600, -2000, and -1000 bar) with respect to the one at 1 bar. b) In dashed black (for 1 bar), green (for -1000 bar), red (for -2000 bar), and blue (for -2600 bar) lines, we present free energy barriers  $\Delta G_c = N_c \cdot \Delta\mu/2$  where  $N_c(\Delta T)$  is given by the common fit of Eq. 7 and for  $\Delta\mu$  we use the corresponding values for each isobar. In solid black line the common fit for  $\Delta G_c$  proposed in Eq. 8 and in turquoise the fit for 2000 bar from Ref. [7]. As black circles we show the data in the -2600 bar  $< p < 450$  bar regime, where solid circles are computed in this work and empty come from Refs. [7, 21].

## B. Interfacial free energy and melting line of the ice Ih-water interface

We now understand the small variability with pressure of the nucleation properties as a function of supercooling at negative and moderate pressure. In order to understand why  $\gamma_m$  displays a shallow minimum, we use the thermodynamic formalism of Gibbs for interfaces [49, 64]. The interfacial Gibbs-Duhem relation is given by,

$$d\gamma_m = -\Gamma d\mu_m - \eta_\gamma dT_m, \quad (10)$$

where  $\Gamma = N_\gamma/A$  is the surface excess density, also called adsorption, and  $\eta_\gamma = S_\gamma/A$  is the excess contribution to

the entropy. Since the location of the dividing surface is arbitrary, excess functions depend also on this choice with the exception of  $\gamma_m$ . For a planar interface,  $\gamma_m$  does not change with the location of the dividing surface unlike in the case of curved interfaces, where  $\gamma$  does change with its location [49, 51, 53]. The choice that most simplifies the thermodynamic treatment in our case is the equimolar dividing surface, usually denoted as the Gibbs dividing surface, where the excess components  $N_\gamma$  is zero, and so is  $\Gamma$  (see Appendix for a general dividing surface treatment). Hence, we can write

$$\frac{d\gamma_m}{dT_m} = -\eta_\gamma^e, \quad (11)$$

where the superscript  $e$  denotes the equimolar dividing surface. Equation 11 provides us with the temperature dependence of the interfacial free energy. It is crucial to note that this derivative must be taken along the co-existence line so that  $p$  is not constant. In fact, we can change Eq. 11 to describe the change of  $\gamma_m$  with pressure along the melting line  $p_m$  as,

$$\frac{d\gamma_m}{dp_m} = -\eta_\gamma^e \frac{dT_m}{dp_m}. \quad (12)$$

In our case, Eq. 12 is more convenient due to the reentrant behavior of the melting curve, i.e. for each  $T_m$  one has two values of  $p_m$  whereas for each  $p_m$  there is only one value of  $T_m$  (see solid red curve in Fig. 3). From Eq. 12, one can see that the change in  $\gamma_m$  with  $p_m$  is determined by the slope of the melting line and the value of the excess entropy per area at the equimolar dividing surface,  $\eta_\gamma^e$ . This means that if there is reentrant behavior for the melting point, there must be reentrant behavior also for  $\gamma_m$  as a function of pressure exactly at the same  $p_m$ , because  $\eta_\gamma^e$  must be finite. In fact, Bianco et al. [21] reported reentrant behavior in the ice Ih-liquid coexistence line of TIP4P/Ice, whose turning point occurred at -2000 bar.

Next, we want to confirm that the maximum in the melting line  $T_m(p_m)$  is consistent with the minimum in  $\gamma_m(p_m)$  that we have obtained from the mold integration technique. Thus, we fit the data for  $\gamma_m(p_m)$  from mold integration with a quadratic fit with the constraint of having the vertex at the same  $p_m$  (-2000 bar) as the quadratic fit for  $T_m(p_m)$ . The latter,  $T_m(p) = a_{T_m}p^2 + b_{T_m}p + c_{T_m}$  has the parameters  $c_{T_m} = 271$  K,  $b_{T_m} = -8.5 \cdot 10^{-3}$  K/bar, and  $a_{T_m} = -2 \cdot 10^{-6}$  K/bar<sup>2</sup>. In this way, we assume that  $\eta_\gamma^e$  is constant. The result is shown in Fig. 6. In the left panel, we show the melting line with points from the direct coexistence simulations of Ref. [21] and the quadratic fit. On the right panel, we show the points of  $\gamma_m$  from mold integration from this work and Ref. [39] as well as the quadratic fit. As can be seen in the right panel, the fit is fairly good even though

we impose constant  $\eta_\gamma^e$  and quadratic fits with the constraint of having the vertex at the same  $p$ . Therefore, assuming that  $\eta_\gamma^e$  is constant seems to be a reasonable approximation.

At this level of approximation,  $\eta_\gamma^e$  is found to be 0.32 mJ/m<sup>2</sup>K. Notice that  $\eta_\gamma^e > 0$  as expected from Eq. 12. For instance, from 1 bar to 2000 bar,  $T_m$  decreases from 270 K to 246.5 K, and  $\gamma_m$  increases from 27.2 mJ/m<sup>2</sup> to 37.2 mJ/m<sup>2</sup>. Therefore,  $d\gamma_m/dp_m > 0$  and  $dT_m/dp_m < 0$ , which means that  $\eta_\gamma^e$  is positive. On the other side of the vertex, from -2600 bar to -2000 bar,  $T_m$  increases from 279 K to 280K while  $\gamma_m$  decreases from 27.1 mJ/m<sup>2</sup> to 26.5 mJ/m<sup>2</sup>. Hence,  $d\gamma_m/dp_m < 0$  and  $dT_m/dp_m > 0$  so that the same sign in  $\eta_\gamma^e$  holds. Notice that Eq. 11 is only valid for planar interfaces along the melting line. If one tries to apply this equation away from of this line as was done in previous works [7, 14, 65], probably one should incorporate terms that account for the change in  $\gamma$  due to curvature. Notice also that the empirical relation proposed by Turnbull which states that  $\gamma_m$  is proportional to the change in melting enthalpy  $\Delta H_m$  does not describe  $\gamma_m$  well at high pressure. From 1 to 2000 bar,  $\Delta H_m$  decreases from 1.44 kcal/mol to almost 1 kcal/mol in experiments [66] and from 1.29 kcal/mol to approximately 1 kcal/mol [67] for the TIP4P/Ice model. Thus, the Turnbull relation predicts a decreasing  $\gamma_m$ , which is not supported by our direct calculations via the mold integration technique.

As can be seen in Fig. 6, the knowledge of the equilibrium melting curve, and the assumption of a constant value for the interfacial excess entropy is sufficient to understand the complex variation of  $\gamma_m$  along the melting line. Another relevant excess variable which depends on  $\gamma_m$ ,  $T_m$ , and  $\eta_\gamma^e$  is the excess energy  $e_\gamma^e$ ,

$$e_\gamma^e = \gamma_m + T_m \eta_\gamma^e. \quad (13)$$

The excess energy  $e_\gamma^e$  is the difference in energy between the actual system having an interface and a virtual system where the two phases remain unchanged up to the dividing surface (the equimolar one in this case). As a result of Eq. 12, the following relation holds,

$$\frac{de_\gamma^e}{dp_m} = T_m \frac{d\eta_\gamma^e}{dp_m}, \quad (14)$$

so that if  $\eta_\gamma^e$  is constant, then  $e_\gamma^e$  must be constant as well. If we approximate  $\eta_\gamma^e$  as constant with the value of 0.32 mJ/m<sup>2</sup>K, we find  $e_\gamma^e = 115$  mJ/m<sup>2</sup>.

#### IV. CONCLUSIONS

In conclusion, we perform seeding simulations to study ice nucleation at negative pressures. Such conditions

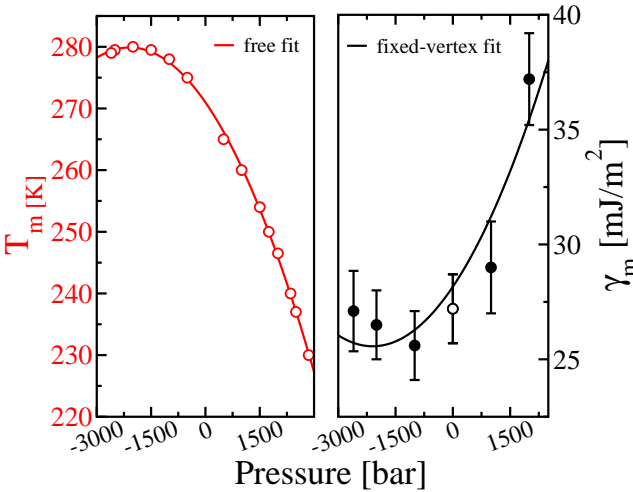


FIG. 6. Left: Melting temperature as a function of pressure. Empty circles are from Ref. [21]. The line is a quadratic fit. Right: Interfacial free energy as a function of pressure. Solid points are from this work and empty points are from Ref. [39]. The line is a quadratic fit constrained to have the vertex at the same pressure (-2000 bar) than the quadratic fit of the left panel.

can be relevant in porous media and water transport in plants, where supercooled water can be at negative pressure. By comparing with previous results, we show that universal empirical expressions describe  $N_c$ ,  $\Delta G_c$ ,  $\gamma$ , and  $J$ , as a function of supercooling for isobars in the regime from strongly negative (-2600 bar) to moderately positive pressures (500 bar). Only when pressure is high (2000 bar), these relations break down. In the regime where pressure hardly plays any role, the isobaric Tolman length is predicted to be positive and roughly constant with the value of 0.24 nm. Also, our results suggest that the homogeneous nucleation line should be parallel to the coexistence line when pressure is below approximately 500 bar (while at higher pressure they are not). We explain this result by inspecting how the interfacial free energy at coexistence changes with pressure. We evaluate the interfacial free energy at coexistence at different states from strongly negative to high pressure by means of the mold integration technique. We show that the interfacial free energy at coexistence barely changes with pressure as long as the system is below 500 bar. In fact, a shallow minimum is reported at negative pressure suggesting that the minimum interfacial free energy between ice Ih and water is around  $26 \pm 1$  mJ/m<sup>2</sup> for the basal plane expanding for a broad range of pressure centered around -2000 bar. Then, we use the Gibbsian formalism to explain that this minimum in the interfacial free energy is connected to a maximum in the melting temperature as a function of pressure. In particular, we show that the change in the interfacial free energy with pressure is proportional to the excess entropy and to the slope of the melting line. Thus, the reentrance in the interfacial free energy occurs because of the reentrance in the melt-

ing line, which happens due to the cross-over in density between ice and water. Finally, we estimate the excess entropy and the excess energy of the ice Ih-water interface. We suggest that a constant value of 0.32 mJ/m<sup>2</sup>K and 115 mJ/m<sup>2</sup> respectively is enough to provide a good description of the thermodynamics of the ice Ih-water interface.

## V. ACKNOWLEDGMENTS

The authors thank Eduardo Sanz and Salvatore Romano for fruitful discussions. PMdH acknowledges support from the SFB TACO (project nr. F81-N) funded by the Austrian Science Fund. JRE acknowledges funding from the Oppenheimer Fellowship, the Roger Ekins Fellowship from Emmanuel College, and a Ramon y Cajal Fellowship (RYC2021-030937-I). CV acknowledges support from project PID2019-105898GB-C21 of the Ministerio de Educacion y Cultura. This work has been performed using resources provided by the Spanish Supercomputing Network (RES), the Vienna Scientific Cluster (VSC), and the Cambridge Tier-2 system operated by the University of Cambridge Research Computing Service (<http://www.hpc.cam.ac.uk>) funded by EPSRC Tier-2 capital grant EP/P020259/1.

## VI. AUTHOR DECLARATIONS

### A. Conflict of Interest

The authors have no conflicts to disclose.

### B. Data availability

The data that support the findings of this study are available from the corresponding author upon reasonable request.

## VII. APPENDIX: INTERFACIAL FREE ENERGY ALONG THE MELTING LINE FOR A GENERAL DIVIDING SURFACE

In this work we used the equimolar dividing surface for simplicity. However, Eqs. 11 and 12 can be generalized for any choice of the dividing surface. To do so, it is necessary to involve not only the interfacial Gibbs-Duhem relation (10), but also the ice and liquid Gibbs-Duhem relations. Respectively, these are,

$$d\mu_m - v_i dp_m + s_i dT_m = 0, \quad (15)$$

$$d\mu_m - v_w dp_m + s_w dT_m = 0, \quad (16)$$

where  $v$  is the volume per molecule (the inverse of the number density) and  $s$  is the entropy per molecule. Since phase equilibrium holds,  $d\mu_m$ ,  $dp_m$ , and  $dT_m$  are common in all phases. Notice that from Eq. 15 and Eq. 16, one can obtain the Clausius-Clapeyron relation that explains the slope of the melting line.

$$\frac{dT_m}{dp_m} = \frac{v_w - v_i}{s_w - s_i}. \quad (17)$$

By including also Eq. 10 in the relation, one can obtain the temperature and pressure dependence of the interfacial free energy without imposing a specific dividing surface. For the temperature, one obtains,

$$\frac{d\gamma_m}{dT_m} = \left[ \Gamma \frac{v_w s_i - v_i s_w}{v_w - v_i} - \eta_\gamma \right], \quad (18)$$

whereas for the pressure, one finds

$$\frac{d\gamma_m}{dp_m} = \left[ \Gamma \frac{v_w s_i - v_i s_w}{v_w - v_i} - \eta_\gamma \right] \frac{dT_m}{dp_m}. \quad (19)$$

As can be seen, at the equimolar dividing surface where  $\Gamma = 0$ , one recovers Eq. 11 and Eq. 12 respectively. These expressions are relevant when nucleation data are extrapolated to coexistence because the relevant dividing surface in nucleation is usually the surface of tension for which  $\Gamma \neq 0$ .

---

[1] R. Geidobler and G. Winter, European Journal of Pharmaceutics and Biopharmaceutics **85**, 214 (2013).

[2] X. Xue, H.-L. Jin, Z.-Z. He, and J. Liu, Journal of Heat Transfer **137**, 091020 (2015).

[3] D. E. Pegg, Preservation of Human oocytes CRC Press (2009).

[4] H. Kanno, R. Speedy, and C. Angell, Science **189**, 880 (1975).

[5] M. Kalichevsky, D. Knorr, and P. Lillford, Trends in Food Science & Technology **6**, 253 (1995).

[6] M. N. Martino, L. Otero, P. Sanz, and N. Zaritzky, Meat Science **50**, 303 (1998).

[7] J. R. Espinosa, A. Zaragoza, P. Rosales-Pelaez, C. Navarro, C. Valeriani, C. Vega, and E. Sanz, Physical Review Letters **117**, 135702 (2016).

[8] R. C. Tolman, The journal of Chemical Physics **17**, 333 (1949).

[9] E. Sanz, C. Vega, J. Espinosa, R. Caballero-Bernal, J. Abascal, and C. Valeriani, Journal of the American Chemical Society **135**, 15008 (2013).

[10] T. Koop, B. Luo, A. Tsias, and T. Peter, Nature **406**, 611 (2000).

[11] J. Espinosa, E. Sanz, C. Valeriani, and C. Vega, The Journal of Chemical Physics **141**, 18C529 (2014).

[12] H. Niu, Y. I. Yang, and M. Parrinello, Physical Review Letters **122**, 245501 (2019).

[13] J. Espinosa, C. Navarro, E. Sanz, C. Valeriani, and C. Vega, The Journal of Chemical Physics **145**, 211922 (2016).

[14] P. M. Piaggi, J. Weis, A. Z. Panagiotopoulos, P. G. Debenedetti, and R. Car, Proceedings of the National Academy of Sciences **119** (2022).

[15] T. Li, D. Donadio, G. Russo, and G. Galli, Physical Chemistry Chemical Physics **13**, 19807 (2011).

[16] H. Laksmono, T. A. McQueen, J. A. Sellberg, N. D. Loh, C. Huang, D. Schlesinger, R. G. Sierra, C. Y. Hampton, D. Nordlund, M. Beye, *et al.*, The Journal of Physical Chemistry Letters **6**, 2826 (2015).

[17] A. J. Amaya and B. E. Wyslouzil, The Journal of Chemical Physics **148**, 084501 (2018).

[18] C. Jeffery and P. Austin, Journal of Geophysical Research: Atmospheres **102**, 25269 (1997).

[19] B. Cheng, C. Dellago, and M. Ceriotti, Physical Chemistry Chemical Physics **20**, 28732 (2018).

[20] C. Marcolli, Scientific reports **7**, 1 (2017).

[21] V. Bianco, P. M. de Higes, C. P. Lamas, E. Sanz, and C. Vega, Physical Review Letters **126**, 015704 (2021).

[22] E. Rosky, W. Cantrell, T. Li, and R. A. Shaw, Chemical Physics Letters **789**, 139289 (2022).

[23] E. Roedder, Science **155**, 1413 (1967).

[24] T. D. Wheeler and A. D. Stroock, Nature **455**, 208 (2008).

[25] F. Caupin, A. Arvengas, K. Davitt, M. E. M. Azouzi, K. I. Shmulovich, C. Ramboz, D. A. Sessoms, and A. D. Stroock, Journal of Physics: Condensed Matter **24**, 284110 (2012).

[26] P. G. Debenedetti, in *Metastable Liquids* (Princeton university press, 2021).

[27] A. R. Imre, Physica status solidi (b) **244**, 893 (2007).

[28] G. Menzl, M. A. Gonzalez, P. Geiger, F. Caupin, J. L. Abascal, C. Valeriani, and C. Dellago, Proceedings of the National Academy of Sciences **113**, 13582 (2016).

[29] F. Caupin and E. Herbert, Comptes Rendus Physique **7**, 1000 (2006).

[30] S. Henderson and R. Speedy, Journal of Physics E: Scientific Instruments **13**, 778 (1980).

[31] L. J. Briggs, Journal of Applied Physics **21**, 721 (1950).

[32] K. Davitt, E. Rolley, F. Caupin, A. Arvengas, and S. Balibar, The Journal of Chemical Physics **133**, 174507 (2010).

[33] J. Abascal, E. Sanz, R. García Fernández, and C. Vega, The Journal of Chemical Physics **122**, 234511 (2005).

[34] V. C. Weiss, M. Rullich, C. Köhler, and T. Frauenheim, The Journal of Chemical Physics **135**, 034701 (2011).

[35] P. Montero de Higes, J. Espinosa, C. Vega, and E. Sanz, The Journal of Chemical Physics **151**, 044509 (2019).

[36] P. G. Debenedetti, F. Sciortino, and G. H. Zerze, Science **369**, 289 (2020).

[37] L. Lupi, B. Vázquez Ramírez, and P. Gallo, The Journal of Chemical Physics **155**, 054502 (2021).

[38] J. R. Espinosa, C. Vega, C. Valeriani, and E. Sanz, *The Journal of Chemical Physics* **144**, 034501 (2016).

[39] J. R. Espinosa, C. Vega, and E. Sanz, *The Journal of Physical Chemistry C* **120**, 8068 (2016).

[40] S. Nosé, *The Journal of Chemical Physics* **81**, 511 (1984).

[41] W. G. Hoover, *Physical review A* **31**, 1695 (1985).

[42] M. Parrinello and A. Rahman, *Physical Review Letters* **45**, 1196 (1980).

[43] U. Essmann, L. Perera, M. L. Berkowitz, T. Darden, H. Lee, and L. G. Pedersen, *The Journal of Chemical Physics* **103**, 8577 (1995).

[44] X. M. Bai and M. Li, *The Journal of Chemical Physics* **122**, 224510 (2005).

[45] B. C. Knott, V. Molinero, M. F. Doherty, and B. Peters, *Journal of the American Chemical Society* **134**, 19544 (2012).

[46] K. F. Kelton and A. L. Greer, *Nucleation in condensed matter: applications in materials and biology* (Elsevier, 2010).

[47] D. Kashchiev, *Nucleation* (Elsevier, 2000).

[48] S. Kondo, *The Journal of Chemical Physics* **25**, 662 (1956).

[49] J. S. Rowlinson and B. Widom, *Molecular theory of capillarity* (Courier Corporation, 2013).

[50] A. Tröster, M. Oettel, B. Block, P. Virnau, and K. Binder, *The Journal of Chemical Physics* **136**, 064709 (2012).

[51] P. Montero de Higes, K. Shi, E. G. Noya, E. Santiso, K. Gubbins, E. Sanz, and C. Vega, *The Journal of Chemical Physics* **153**, 191102 (2020).

[52] D. Kashchiev, *The Journal of Chemical Physics* **153**, 124509 (2020).

[53] P. Montero de Higes and C. Vega, *The Journal of Chemical Physics* **156**, 014505 (2022).

[54] P. Montero de Higes, J. R. Espinosa, E. Sanz, and C. Vega, *The Journal of Chemical Physics* **151**, 144501 (2019).

[55] J. R. Espinosa, G. D. Soria, J. Ramirez, C. Valeriani, C. Vega, and E. Sanz, *The Journal of Physical Chemistry Letters* **8**, 4486 (2017).

[56] W. Lechner and C. Dellago, *The Journal of Chemical Physics* **129**, 114707 (2008).

[57] C. Vega, E. Sanz, J. Abascal, and E. Noya, *Journal of Physics: Condensed Matter* **20**, 153101 (2008).

[58] J. W. Schmelzer, A. S. Abyzov, and V. G. Baidakov, *Entropy* **21**, 670 (2019).

[59] V. G. Baidakov and K. R. Protsenko, *The Journal of Physical Chemistry B* **123**, 8103 (2019).

[60] V. Molinero and E. B. Moore, *The Journal of Physical Chemistry B* **113**, 4008 (2009).

[61] R. Handel, R. L. Davidchack, J. Anwar, and A. Brukhno, *Physical Review Letters* **100**, 036104 (2008).

[62] R. L. Davidchack, R. Handel, J. Anwar, and A. V. Brukhno, *Journal of Chemical Theory and Computation* **8**, 2383 (2012).

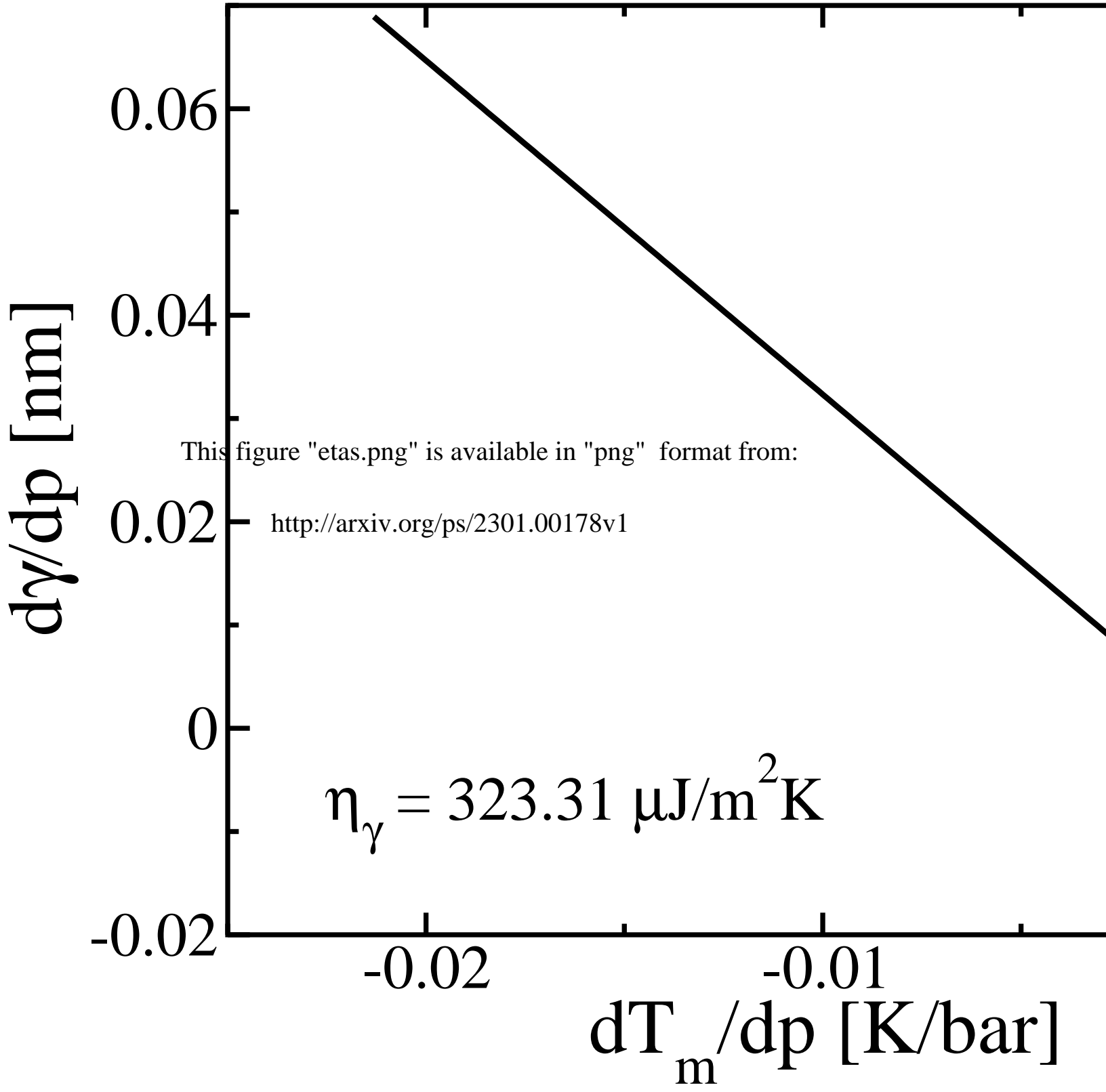
[63] D. Rozmanov and P. G. Kusalik, *The Journal of chemical physics* **137**, 094702 (2012).

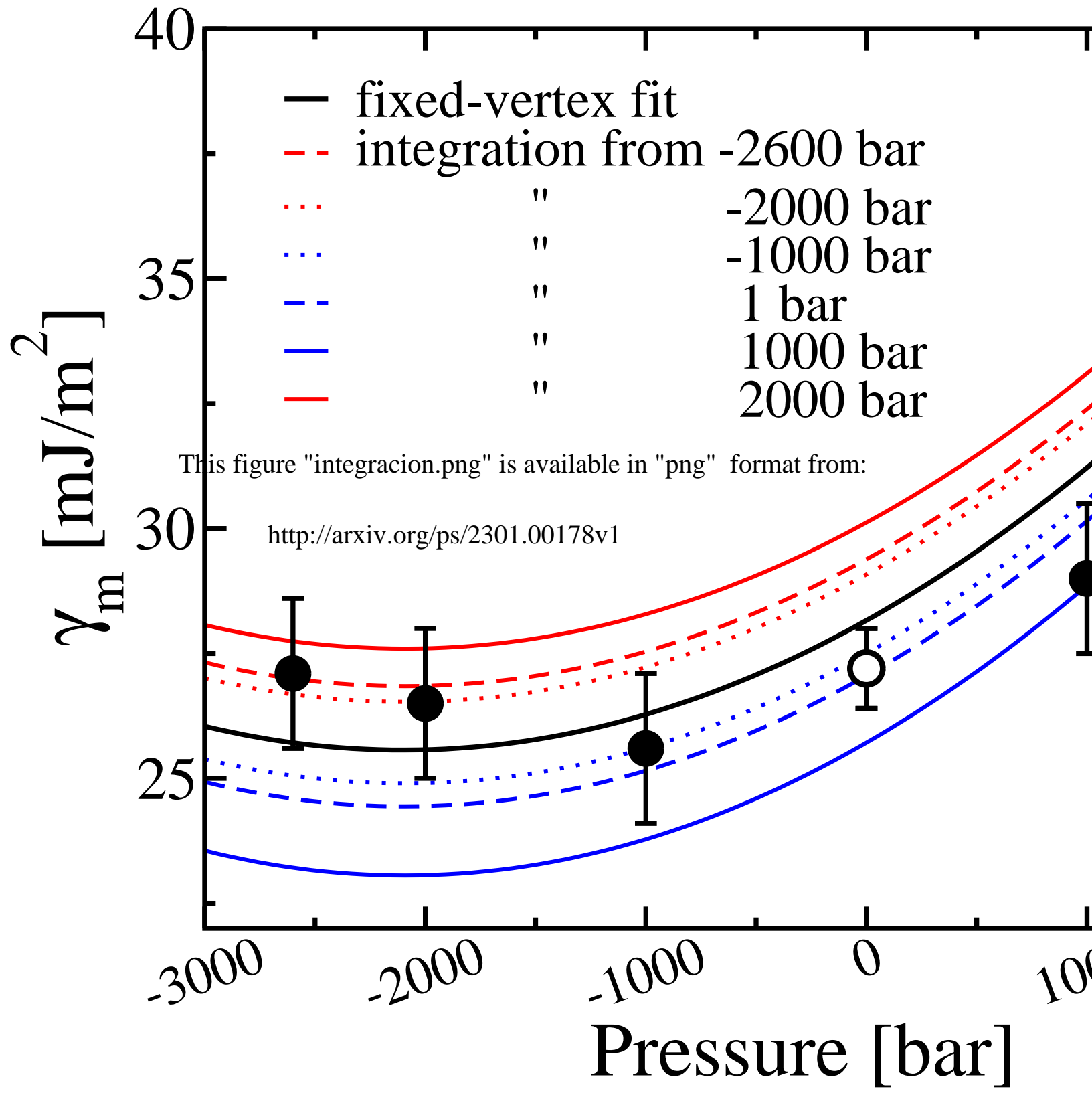
[64] J. W. Gibbs, *The collected works of J. Willard Gibbs, volume I: thermodynamics* (Yale University Press, 1928).

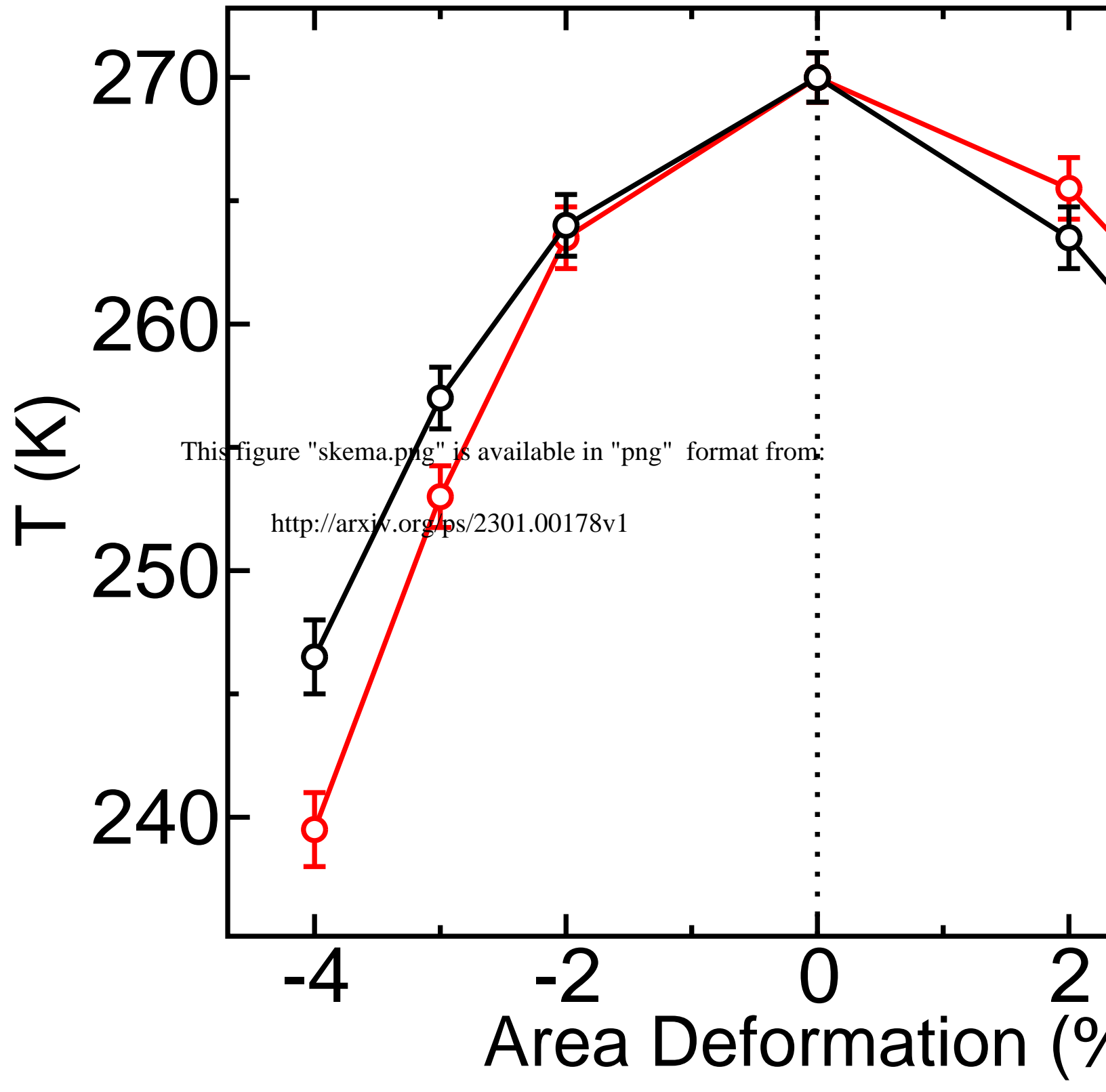
[65] Y. Qiu, L. Lupi, and V. Molinero, *The Journal of Physical Chemistry B* **122**, 3626 (2018).

[66] D. Eisenberg and W. Kauzmann, *The structure and properties of water* (OUP Oxford, 2005).

[67] J. L. Abascal, E. Sanz, and C. Vega, *Physical Chemistry Chemical Physics* **11**, 556 (2009).







This figure "sketi.png" is available in "png" format from:

<http://arxiv.org/ps/2301.00178v1>

This figure "sketii.png" is available in "png" format from:

<http://arxiv.org/ps/2301.00178v1>